01 Jan 2020

Bending Behavior and Deflection Prediction of High-Strength SFRC Beams under Fatigue Loading

Dan Ying Gao

Zhi Qiang Gu

Chenglin Wu
Missouri University of Science and Technology, wuch@mst.edu

Recommended Citation

D. Y. Gao et al., "Bending Behavior and Deflection Prediction of High-Strength SFRC Beams under Fatigue Loading," *Journal of Materials Research and Technology*, vol. 9, no. 3, pp. 6143-6159, Elsevier, Jan 2020. The definitive version is available at https://doi.org/10.1016/j.jmrt.2020.04.017

Available online at www.sciencedirect.com

jmr&t Journal of Materials Research and Technology

www.jmrt.com.br

Original Article

Bending Behavior and Deflection Prediction of High-Strength SFRC Beams under Fatigue Loading

Dan-ying Gao[a,b], *Zhi-qiang Gu*[a,*], *Chenglin Wu*[c,*]

[a] *School of Water Conservancy and Engineering, Zhengzhou University, Zhengzhou, 450001, China*
[b] *Henan University of Engineering, Zhengzhou, 451191, China*
[c] *Department of Civil, Architectural, and Environmental Engineering, Missouri University of Science and Technology, Rolla, 65401, USA*

ARTICLE INFO

Article history:
Received 10 February 2020
Accepted 6 April 2020
Available online 19 April 2020

Keywords:
High-strength SFRC beams
Stress level
Fiber volume fraction
Steel bar strength
Fatigue performance
Deflection prediction

ABSTRACT

The experiments of high-strength steel-fiber-reinforced concrete (SFRC) beams subjected to fatigue bend loading were conducted in this work. A total of 12 beams were tested to failure, including 2 under static loading and 10 under fatigue loading. The main varying parameters of the tested beams included the stress level, fiber volume fraction, and strength of the steel reinforcement. The fatigue life, mid-span deflection, residual deflection, and crack width were measured and evaluated. The stiffness degradation of high-strength SFRC beams was analyzed. The results indicated that both the stress level and fiber volume fraction have significant influences on the fatigue life of the tested beam. The fatigue life of the beams decreased with increasing stress level and increased with fiber volume fraction. With added steel fibers, the stiffness of the beam improved significantly, which leads to the reduced deflection and narrower average crack width during the fatigue loading. The total deflection of high-strength SFRC beam subjected to fatigue loading can be divided into two parts: residual deflections and instantaneous deflections. Both of them were fitted based on the experimental results. Finally, an analytical method which considers the influences of steel fibers was proposed to predict the mid-span deflections of high-strength SFRC beam at different cycles, which agrees well with the experimental results.

1. Introduction

Steel-fiber-reinforced concrete (SFRC) structures can exhibit much improved tensile strength and ductility [1–7]. Existing researches have been demonstrated that the bridging action of steel fibers could transfer tensile stress across cracks, thus restraining crack development and stiffness degradation. With the addition of steel fibers, the punching shear capacity of concrete panel enhanced greatly [1]. Compared to non-fiber-reinforced concrete, SFRC presents the increased toughness and strain at the peak stress, the compressive and ultimate flexural strengths increased both with the increase of fiber content [2,5]. Sufficient addition of steel fibers to concrete could decreasing crack widths and increasing number of cracks [4]. Furthermore, the impact resistance of concrete

* *Corresponding author.*
E-mails: zqgzzu@163.com (Z. Gu), wuch@mst.edu (C. Wu).
https://doi.org/10.1016/j.jmrt.2020.04.017

structure was improved with the addition of high carbon content steel fiber [3,6,7]; the addition of 2% (by volume) steel fibers was effective in decreasing the maximum and residual deflections by impact, improving residual capacities after impact damage [6]; the beams without fiber reinforcement failed by brittle shear under impact load, while the use of 1.0% fiber amount leads to ductile flexure-governed failure [7]. Balázs and Kovács [8] designed 21 fiber-reinforced concrete beams to study their flexural and shear behavior, the experimental results demonstrated that steel fibers not only decrease the average crack width but also provide substantial post-peak resistance and ductility for conventional reinforced concrete members. Meda et al. [9] also reported fibers could improve the service performance by limiting the crack development and increasing stiffness in the post-cracking stage.

The fatigue performances of SFRC also received much attention. Yin and Hsu [10] studied the fatigue performance of plain and fiber concrete in uniaxial and biaxial compression. Results showed that adding steel fibers to concrete can significantly improve the ductility of specimen subjected uniaxial cyclic loading. In addition, the fatigue strength of SFRC has shown a drastic increase when undergoing high levels of stress. Cachim et al. [11] also found that SFRC presented a greater deformation than plain concrete at failure under fatigue loading. Compared with the fatigue performance under compressive fatigue loading, SFRC showed a better performance under flexural fatigue loading [12]. Since the crack bridging action of steel fibers under tensile region, the fatigue life of concrete structure was extended [13,14].

All of above researches indicated that adding steel fibers to concrete can significantly improve the fatigue behavior of SFRC under cyclic loading. However, these experiments were all conducted for the small scale specimens without steel reinforcement, the fatigue behavior of large scale SFRC structures reinforced with steel bars such as bridge decks, crane beams, airport pavements, and railway foundations has not been fully investigated, yet critical to their durability and safety [15]. Gao et al. [16] designed 13 SFRC beams subjected to fatigue loading, the stress level, fiber content, fiber type, and reinforcement strength were considered in this research. Parvez and Foster [17] designed 16 SFRC beams with different fiber contents and component sizes, and tested them under fatigue loading. The results, concluded from the above researches, showed that the fatigue life of beams is prolonged with the addition of steel fibers. The SFRC beams showed the lower deflections and smaller crack widths during the loading process compared to non-fiber-reinforced concrete beams. The rate of stiffness degradation of specimens was reduced with the addition of steel fibers. In addition, there is an increasing interest in combining the high strength reinforcement bars with fiber-reinforced concrete in the engineering, especially for slender structures with strict deflection requirements [18–21]. As one of the most important parameters to evaluate the structural behaviors, the deflection prediction of reinforced concrete beam under static condition has been widely investigated [22–24] and already introduced to the American Concrete Institute code [25]. However, the deflection evolution has not been systematically investigated for SFRC beams under fatigue condition, which is critical to their long-term durability performance and associated design criterion.

The deflection development of beams under fatigue loading is a complex process, which is determined by many factors including the applied loading, the bond-slip between concrete and steel bar, and the creep of concrete under long-term fatigue loading. CEB-FIP [26] proposed a simplified empirical formula to predict the beam deflections under fatigue loading. However, this empirical equation lacks physical failure mechanism which could omit unexpected failure modes. In addition, it does not consider the influence of the fiber reinforcement on the fatigue deflection. Currently, only numerical predictions on the fatigue behavior of SFRC beams were conducted [27], the analytical model for deflection prediction of SFRC under fatigue loading is desperately needed to provide the foundation for a mechanism-based rational design.

In this work, 12 high-strength SFRC beams were tested under static and fatigue loading, the mid-span deflection and residual deflection were measured using linear variable differential transformers during the fatigue loading. Furthermore, the crack propagation and crack width were monitored at fixed fatigue cycles. Based on the experimental results, an analytical model considering the fiber influences was proposed to predict the mid-span deflections under fatigue loading. This model firstly calculated the deflections of high-strength SFRC beam in the first cycle under static loading, and the influences of steel fiber on the beam stiffness was considered based on an effective moment of inertia method. Then, the residual deflection and instantaneous deflection under fatigue loading were studied, the analytical formula which considered the fiber influence was proposed to obtain reliable predictions. The model can predict the residual deflections and total deflections of high-strength SFRC beam at any number of fatigue cycles. The predicted deflection responses closely agree with the experimental results, which validates the proposed model. In addition, the analysis also lays a foundation for a mechanism-based fatigue design approach for high-strength SFRC beam structures.

2. Experimental program

2.1. *Materials*

The targeted compressive strength of concrete was designed as 80 MPa. Gravel with the average particle size of 12.5 mm and river sand with a maximum particle size of 5 mm were used as coarse and fine aggregates, respectively. Portland cement was used as cementitious materials with a strength of 42.5 MPa. A polycarboxylate superplasticizer with a water-reducing rate of 20% was used to improve the workability of concrete. The mix proportion of concrete was 1:1.2:2.1:0.008 (cement: river sand: coarse aggregate: superplasticizer by weight) with a water/cement ratio of 0.31. Hooked-end steel fibers with volume contents of 0.5%, 1.0%, and 1.5% were added into the concrete. The steel fiber has an ultimate tensile strength of 1345 MPa and elastic modulus of 200 GPa. The size and shape of the fibers are presented in Fig. 1. Four types of steel bars used in this experimental program were: 12 mm diameter deformed bars with the yield strength of 400 MPa (HRB400), 500 MPa (HRB500) and 600 MPa (HRB600), and 8 mm plain bars

Table 1 – Properties of steel bars.

Reinforcement type	Diameter (mm)	Yield strength (MPa)	Tensile strength (MPa)	Elastic modulus (MPa)	Elongation (%)
HRB400	12	498	648	2.0×10^5	23
HRB500	12	585	705	2.05×10^5	22
HRB600	12	637	828	2.0×10^5	19.3
HPB300	8	425	550	1.87×10^5	28.5

Table 2 – Test program.

Specimens ID	Test type	Fiber volume fraction (%)	Tensile reinforcement strength	Stress level (P_{max}/P_u)	Applied load	
					P_{max} (kN)	P_{min} (kN)
BJ1.0-4	Static	1.0	HRB400	—	—	—
BJ1.0-5	Static	1.0	HRB500	—	—	—
BS1.0-5	Fatigue	1.0	HRB500	0.5	97.8	19.6
BS1.0-55	Fatigue	1.0	HRB500	0.55	107.6	19.6
BS1.0-6	Fatigue	1.0	HRB500	0.6	117.4	19.6
BS1.0-7	Fatigue	1.0	HRB500	0.7	136.9	19.6
BS1.0-8	Fatigue	1.0	HRB500	0.8	156.5	19.6
BF0-6	Fatigue	0	HRB500	0.6	107.4	17.9
BF0.5-6	Fatigue	0.5	HRB500	0.6	111	18.5
BF1.5-6	Fatigue	1.5	HRB500	0.6	122.3	20.4
BH1.0-4	Fatigue	1.0	HRB400	0.6	101.3	16.9
BH1.0-6	Fatigue	1.0	HRB600	0.6	132.8	22.1

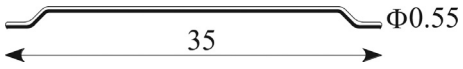

Fig. 1 – Dimensions and shape of steel fiber (units: mm).

with the yield strength of 300 MPa (HPB300). The mechanical properties of the reinforcement bars are listed in Table 1.

2.2. *Test specimens*

The experiments consisted of 12 high-strength SFRC beams as listed in Table 2. All beams were 1200 mm long, with a constant section area of 120 mm (width) × 200 mm (height). Two 12-mm-diameter deformed bars were used as the tensile reinforcement. 8-mm-diameter plain bars with the yielding strength of 300 MPa (HPB300) were used as the compression and shear reinforcement. The stirrups were spaced at 100 mm over the length of the beam. The reinforcement details are presented in Fig. 2. The beams were cast in pairs along with 6 cubes and 6 prisms. Two beams (BJ1.0-4 and BJ1.0-5) with the tensile reinforcement of HRB400 and HRB500 were tested respectively under static loading to determine the ultimate bearing capacity (P_u). The other ten beams tested under fatigue loading were divided into three groups. The first group of beams with HRB500 steel bars and fiber content of 1.0% (BS1.0-5, BS1.0-55, BS1.0-6, BS1.0-7, and BS1.0-8) were tested at different stress levels S_{max} ($S_{max} = P_{max}/P_u$, P_{max} is the maximum fatigue load applied to the beam, P_u is the ultimate bearing capacity of each beam) of 0.5, 0.55, 0.6, 0.7, and 0.8. The second group of beams with HRB500 steel bars and different fiber contents of 0, 0.5%, 1.0%, and 1.5% (BF0-6, BF0.5-6, BS1.0-6, and BF1.5-6) were conducted at the same stress level of 0.6. The third group of beams with a fiber content of 1.0% and different tensile reinforcements of HRB400, HRB500, and HRB600 (BH1.0-4, BS1.0-6, and BH1.0-6) were tested at the stress level of 0.6. The ratio of the minimum fatigue load to the ultimate bearing capacity of each beam S_{min} ($S_{min} = P_{min}/P_u$, P_{min} is the minimum fatigue load applied to the beam) was set as 10%.

2.3. *Test procedure and instrumentation*

All of the beams were conducted under four-point-bend loading with a clear span of 1000 mm, as shown in Fig. 2. The tests were conducted on 500 kN MTS testing machine (244.41, MN USA®). Five LVDTs were used to measure the deflections. One

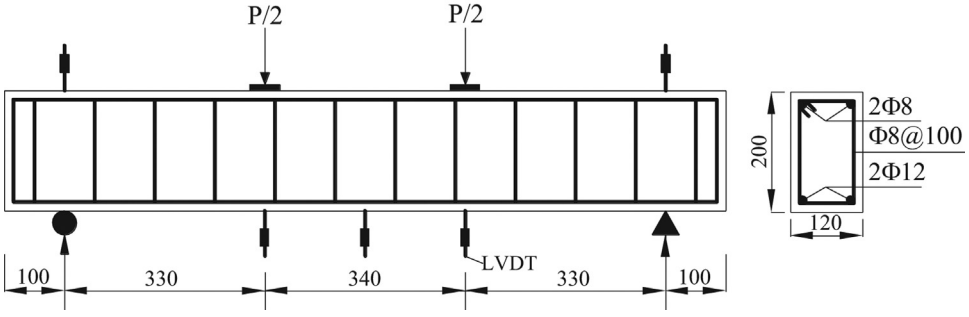

Fig. 2 – Reinforcement details and instruments layout (units: mm).

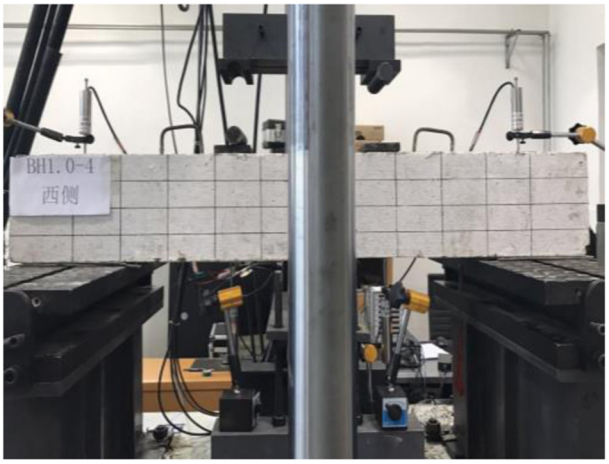

Fig. 3 – Test setup.

of them was installed at the mid-span, two were installed at the loading points, and the last two were installed at the supports. The instrumentation and test setup are shown in Figs. 2 and 3.

The beams BJ1.0-4 and BJ1.0-5 were tested under static loading to determine the ultimate capacity prior to the fatigue loading. A displacement-controlled loading was implemented at a rate of 0.2 mm/min during the static test. A force-controlled loading protocol was implemented for the fatigue tests, as presented in Fig. 4. The beams were loaded to the upper limit of the fatigue load at the first cycle, and then reduced to zero to measure the residual deflection. Subsequently, the fatigue load was applied for a specific number of cycles (N). The static loading rate for the first cycle was 0.2 kN/s and the fatigue loads were applied with a frequency of 5 Hz. Static load tests were conducted alternately at $N = 1 \times 10^3$, 3×10^3, 5×10^3, 1×10^4, 1.5×10^4, 2×10^4, 5×10^4, 1×10^5 and every 10^5 cycles up to specimen's failure. During each static test, the fatigue load was uninstalled to zero and the residual deflections were measured. If the fatigue life exceeded 2 million cycles, the beams were considered as run-out and a static load was applied to failure.

A multi-channel dynamic data acquisition device (HPDJ-8825, NANJINGHEPU®) with an acquisition frequency of 100 Hz was used to measure the deflections and residual deflections. During each static test, the crack developments were marked by a maker pen, and the crack widths of the beam at the tensile reinforcement location were measured by a crack width detector (ZBL-F130). As shown in Fig. 5, the crack width detector has an optical microscope which is connected with the mobile phone. During the test, the optical microscope placed at the crack position of the concrete surface, and the crack width can be displayed on the phone screen precisely.

3. Experimental results and analysis

3.1. *Fatigue life, failure mode, and concrete properties of the beam*

The concrete properties, fatigue life, and failure mode of each beam were listed in Table 3, f_c and E_s are the compressive strength and elastic modulus of concrete, respectively. As shown, the fatigue life of the high-strength SFRC beam decreases with increasing stress level and increases with fiber content. Compared with the beam BS1.0-5 which did not fail after undergoing 2 million cycles under the stress level of 0.5, the fatigue life of the beam under the stress levels of 0.55, 0.6, 0.7, and 0.8 decreased by 56.5%, 60%, 79.6%, and 96.7%, respectively. Furthermore, existing researches had been reported that the applied stresses and fatigue lives of steel reinforcement are well correlated in log-log scales [28,29]. Analyzing the experimental results in this paper, it was found that there also has a good linear relationship between the stress level S_{max} and the logarithm of fatigue life LgN. The expression is given in equation 1 with a correlation coefficient of 0.933.

$$S_{max} = 1.819 - 0.208LgN \quad (1)$$

The fatigue life of the beam with steel fiber volume fractions of 0.5%, 1.0% and 1.5% increased 37.7%, 106.3%, and 61.4% compared to the non-fiber reinforced concrete beam at the same stress level of 0.6, respectively. These improvements show the significant contributions of steel fibers to the increased fatigue life of the beams. The main reason is the fatigue life of under-reinforced concrete beams is governed by both of the tensile strength of reinforcement and concrete,

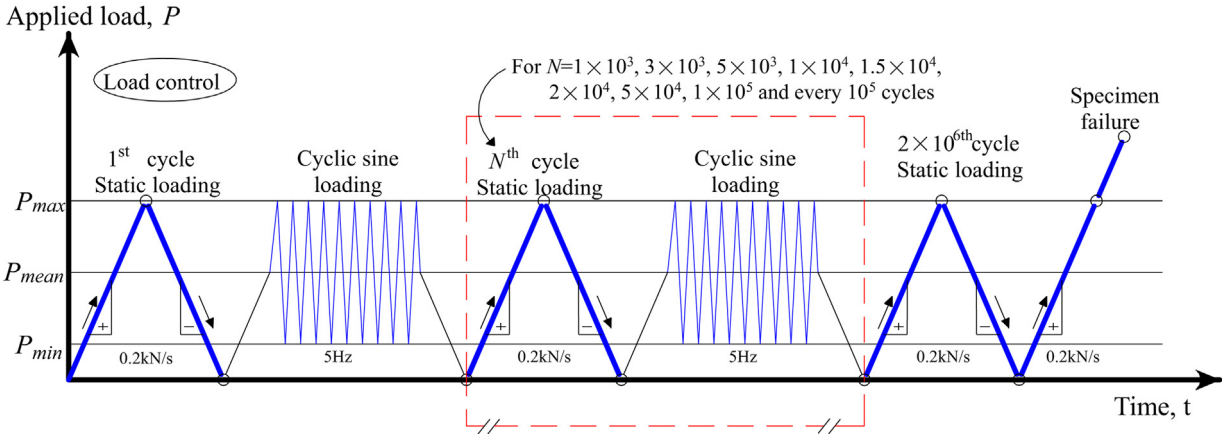

Fig. 4 – Loading system of fatigue test.

Fig. 5 – Crack width detector.

Table 3 – Fatigue life, failure mode, and concrete properties.

Specimens ID	Concrete properties		Fatigue life	Failure mode
	f_c (MPa)	E_c (GPa)		
BJ1.0-4	83.4	40.8	—	Concrete crushing
BJ1.0-5	87.6	41.6	—	Concrete crushing
BS1.0-5	83.4	40.8	>2,000,000	Run-out
BS1.0-55	87.6	41.6	869,751	Steel rupture
BS1.0-6	86.3	42.4	799,389	Steel rupture
BS1.0-7	85.7	39.4	407,724	Steel rupture
BS1.0-8	85.7	39.4	65,296	Steel rupture
BF0-6	75.4	37.1	387,415	Steel rupture
BF0.5-6	79.9	40.8	533,466	Steel rupture
BF1.5-6	85.6	43.2	625,300	Steel rupture
BH1.0-4	83.4	40.8	676,972	Steel rupture
BH1.0-6	87.6	41.6	246,967	Steel rupture

which have been significantly improved by the addition of steel fibers [17]. Obviously, the beam BS1.0-6 with HRB500 steel bars and 1% volume fraction of steel fibers shows the highest fatigue life of 799,389 cycles under the same stress level of 0.6.

3.2. *Failure picture and load-deflection response of the beam failed by static test*

The final failure pictures of the static beams BJ1.0-4 and BJ1.0-5, and beam BS1.0-5 which did not fail after undergoing 2 million fatigue cycles and finally failed by static test, are presented in Fig. 6. In the static test, the deflection increased linearly with the increasing of load during initial stage. When the load increased to nearly 80% of the ultimate capacity of each beam, the tensile reinforcements began to yield, and the load increased gradually while the deflections increased rapidly. At the same time, the steel fibers were pulled out and followed by the initiations of the wide cracks in the specimen. When the beam reached its ultimate bearing capacity, the concrete crushing happened in the compression zone and the load decreased gradually. The beam was regarded as failed when the load decreased to 80% of its ultimate capacity. All of the beams were failed by the concrete crushing in the compression zone, as shown in Fig. 6. The load-deflection curves of these beams are plotted in Fig. 7. As shown, the high-strength SFRC beams show a good ductility in the failure stage, the failure deflections at 80% ultimate capacity are more than five times to the deflections at the ultimate capacity.

3.3. *Failure picture and crack patterns of the beam under fatigue loading*

In the fatigue test, all of the beams were failed by a sudden fracture of the tensile reinforcement (except the beam BS1.0-5 which did not fail after undergoing 2 million fatigue cycles). The final failure pictures and crack patterns of these beams are presented in Fig. 8. In the figure, the blue numbers represent the number of fatigue cycles when the crack develops to this

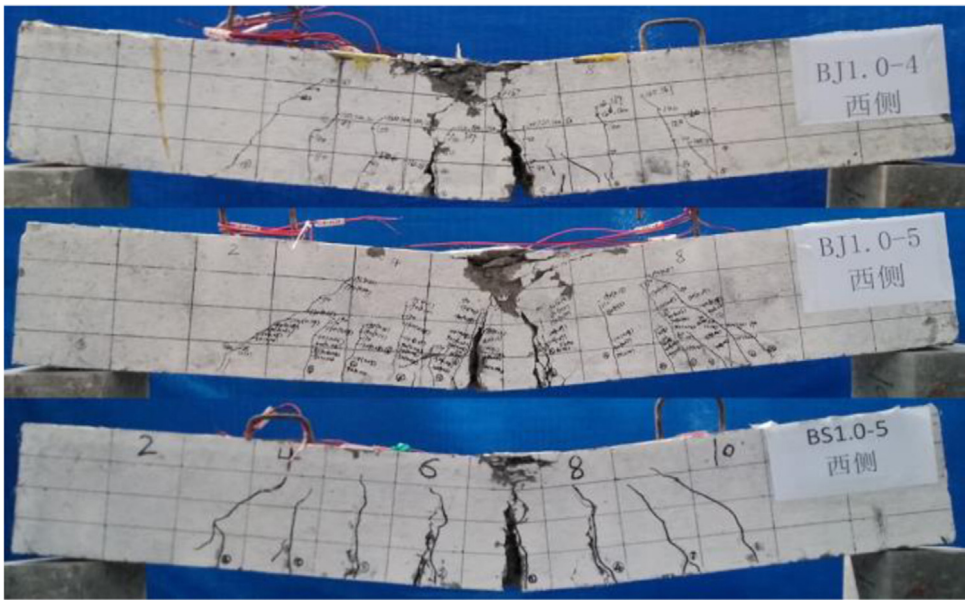

Fig. 6 – Final failure pictures of the beam failed by static test.

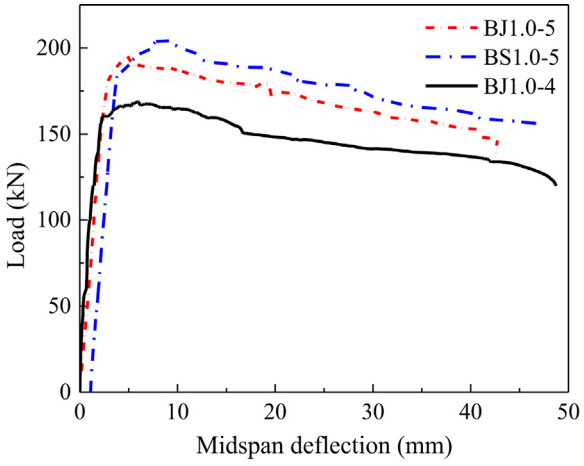

Fig. 7 – Load-deflection curves for static load failure beam.

height, the red lines are the failure locations of the beams, and the circled numbers below the beam indicate the appearance sequence of the cracks under fatigue loading. As shown in Fig. 8, all cracks had almost appeared in the first loading cycles, and the crack widths and heights enlarged with the increase of fatigue cycles. The fatigue damage was accumulated with the increasing fatigue cycles. The stresses of the tensile reinforcement gradually increased as well. When the stresses of the steel bars in the crack locations exceeded the failure strength of the reinforcement, the brittle fracture of beams occurred. The fatigue failure mode of tensile reinforcement in the high-strength SFRC beam is same as the steel reinforcement tested in air [30,31].

3.4. *Maximum and average crack widths of the beam under fatigue loading*

One of the most important advantages for adding steel fibers into concrete is the restrained crack development [32,33], which contributed directly to the enhancement of fatigue life for high-strength SFRC beams. According to the experimental results, the maximum and average crack widths of the beam *versus* the percentage of fatigue life are presented in Fig. 9. Numerous researches had been demonstrated the representative fatigue parameters such as crack width and deflection present three-stage developing pattern *versus* the percentage of fatigue life, both for the single materials such as concrete [34,35] and steel reinforcement [28,36,37], and the composites such as RC structures [38,39]. In this experiment, owing to the crack widths were measured for every 10^5 cycles during each interval, the final stage of the crack development was not captured. So, only the first two stages of the development trend were presented herein.

As shown in Fig. 9a-c, the maximum crack width increases with increasing stress level. The increasing rate of maximum crack width for the beams with fibers is much slower in comparison with those without fiber. In the first stage ($N/N_f < 5\%$), it experiences a rapid increase with the increasing of fatigue cycles. The second stage ($N/N_f \geq 5\%$) of maximum crack width is relatively stable with almost no growth. The evolution of the average crack width follows the same trend as the maximum crack width, as depicted in Fig. 9d-f. However, the first stage ($N/N_f < 10\%$) of the average crack width evolution is a little longer.

The results of average crack widths for the beams with different fiber contents at different fatigue cycles are presented in Table 4. It is observed that the beam with 0.5% fiber volume fraction has shown little reduction in average crack width even at 200,000 cycles compared to non-fiber reinforced concrete beam. For the beams with 1.0% and 1.5% fiber volume fraction,

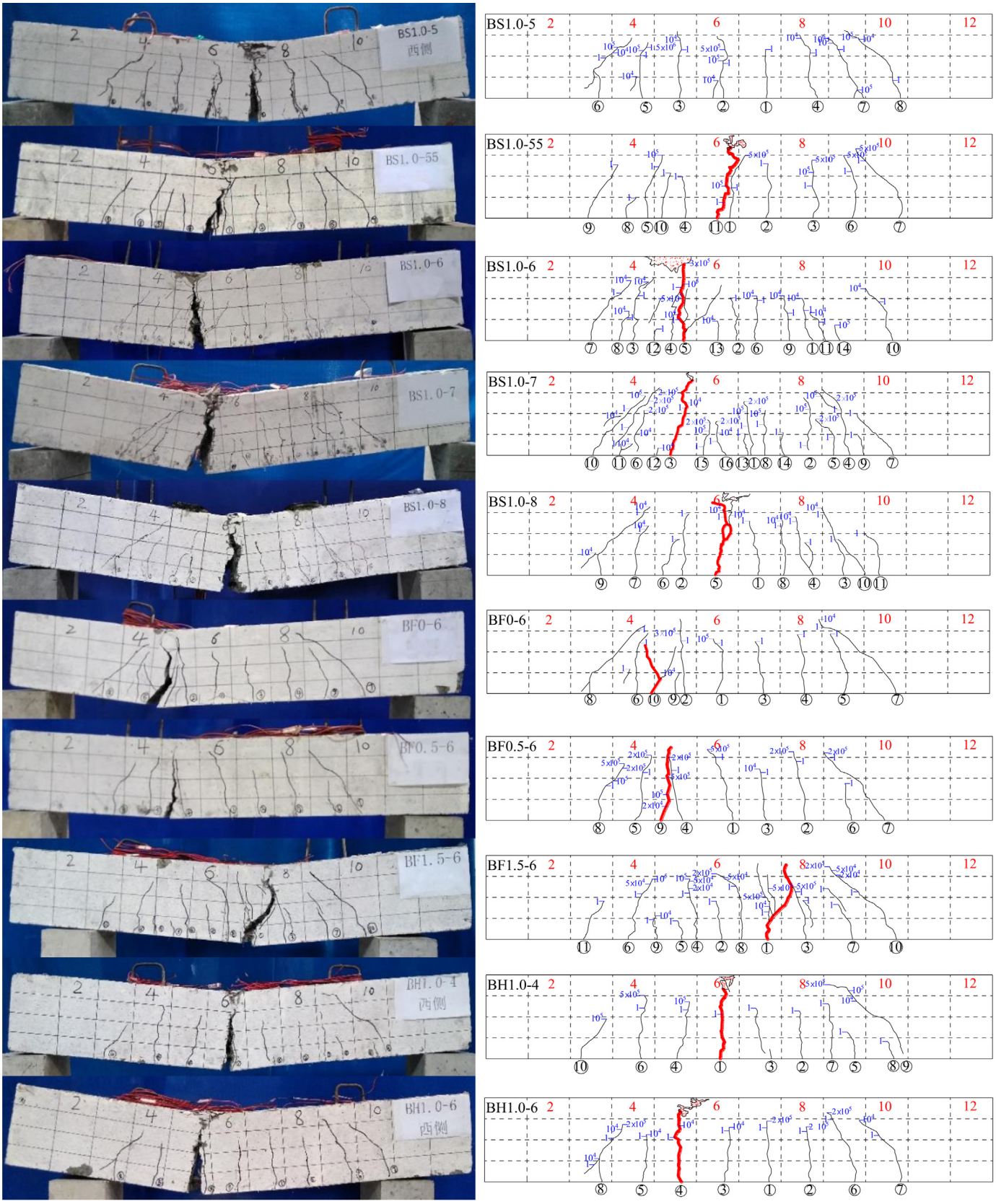

Fig. 8 – Final failure pictures and crack distributions of the beam under fatigue loading.

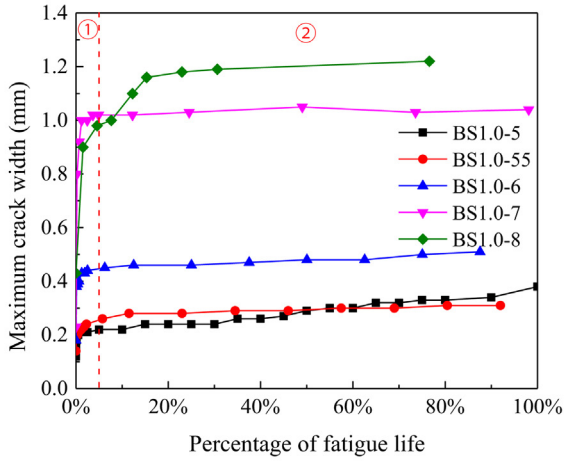

(a) Maximum crack widths at different stress levels

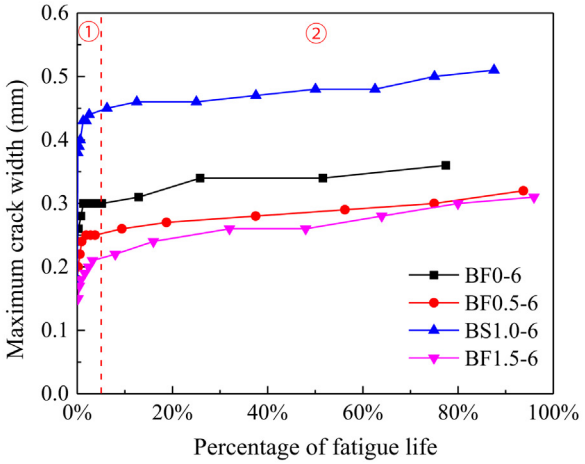

(b) Maximum crack widths at different fiber contents

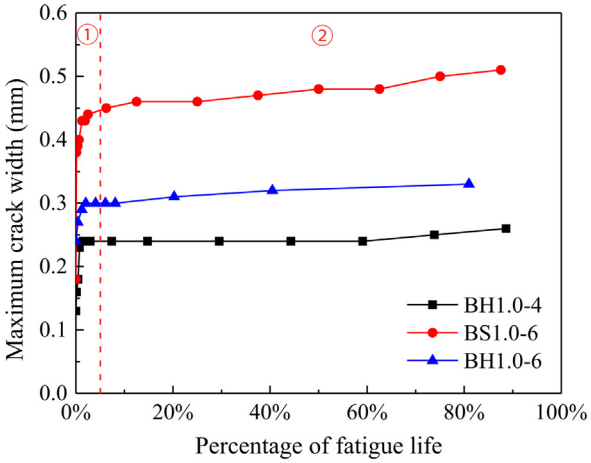

(c) Maximum crack widths at different strengths of tensile reinforcement

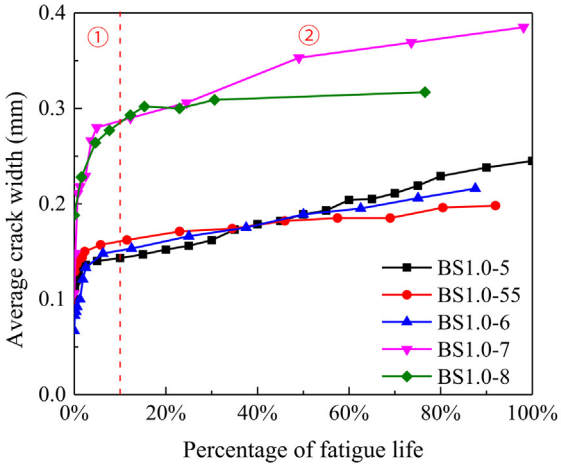

(d) Average crack widths at different stress levels

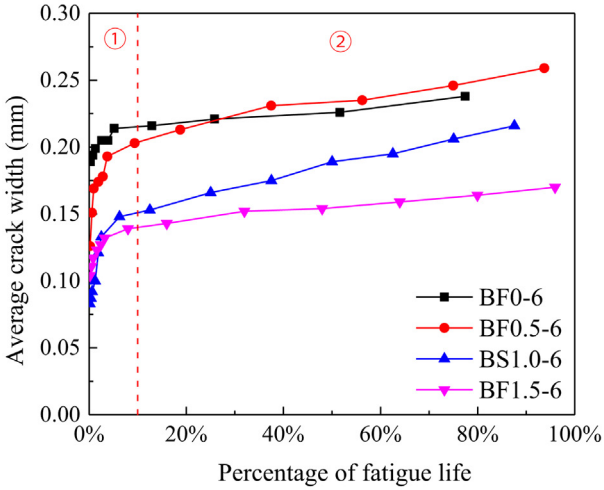

(e) Average crack widths at different fiber contents

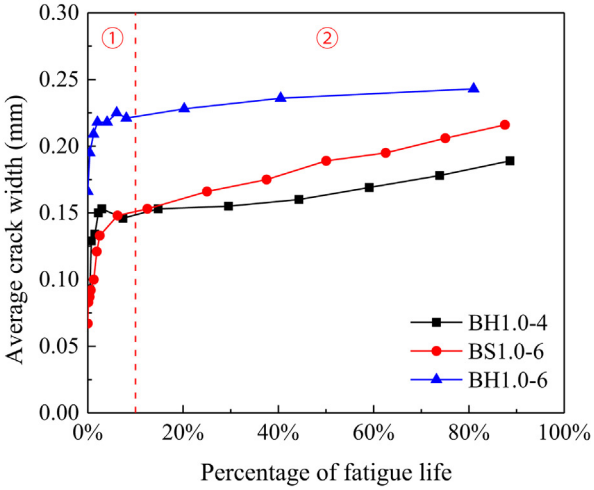

(f) Average crack widths at different strengths of tensile reinforcement

Fig. 9 – Maximum crack widths and average crack widths versus percentage of fatigue life.

Table 4 – Average crack width reduction for series of different fiber content beams.

Specimen ID	At 100,000 cycles		At 200,000 cycles		At 300,000 cycles	
	Average width (mm)	Decrease (%)	Average width (mm)	Decrease (%)	Average width (mm)	Decrease (%)
BF0-6	0.221	-	0.226	-	0.238	-
BF0.5-6	0.213	3.6	0.231	-2.2	0.235	1.3
BS1.0-6	0.153	30.8	0.166	26	0.175	26.5
BF1.5-6	0.143	35.3	0.152	32	0.154	35.3

the average crack width decreases significantly. This indicates a better bonding between rebar and concrete for beams with 1.0% and 1.5% fiber content. It indicates that the fiber contents have a significant effect on the crack width of the beams under fatigue loading due to the enhanced tensile strength of the concrete through the addition of steel fibers, which allows more stress transferring from the rebar to concrete, finally leads to the increasing of crack numbers and the decreasing of average crack widths and maximum crack widths.

3.5. *Deflections and residual deflections of the beam under fatigue loading*

In this experiment, the multi-channel dynamic data acquisition device worked continuously to record the deflection data of the beam under fatigue loading. The maximum deflections under upper limit fatigue load and residual deflections *versus* the percentage of fatigue life for each beam are presented in Fig. 10. As discussed above, the development of maximum and residual deflections for all the beams with the increasing of fatigue life is characterized by three stages. In the first stage of $N/N_f < 10\%$, the deflections increase rapidly with the increasing of fatigue cycles. Then, a stable development stage of maximum deflection and residual deflection begins and the deflection of beams increases gradually, which is named as the second stage with $10\% \leq N/N_f < 90\%$, and accounts for about 80% of whole fatigue life. In third stage with $N/N_f \geq 90\%$, the maximum deflection and residual deflection enter into the unstable stage, the deflection of beams increases significantly until the beam fails in brittle fracture.

It can also be observed from Fig. 10 that the maximum and residual deflections increase with increasing stress level and decrease with fiber content, which has the same tendency as that of the crack widths. This is mainly owing to the addition of steel fibers, which contributes to the enhanced tensile strength of the concrete that eventually increases the stiffness of the beam. Therefore, the effects of steel fiber should be considered in the deflection calculation of SFRC beam subjected to fatigue loading. The residual deflection, which can be defined as the unrecoverable part of fatigue deformation and represents the damage degree of the beam subjected to fatigue loading, is also an important index to evaluate the accumulation of internal defects in the beam. The results of the residual deflection measured in the experiment also confirmed the reduced fatigue damages by introducing the steel fibers. Taking an instant data for different fiber contents group at 50,000 cycles, the residual deflections of high-strength SFRC beams with 0.5%, 1.0%, and 1.5% volume of fiber were 12.8%, 23.5%, and 39.6% less than that of non-fiber reinforced beam, respectively. The bridging stress of steel fiber enhances the bond stress between SFRC and steel bars, thus reduces the bond-slip under fatigue loading, and the internal damage of concrete is also reduced.

3.6. *Flexural Stiffness degradation analysis of the beam under fatigue loading*

According to the theory of mechanics of materials, the flexural stiffness of beam under four-point-bend loading is calculated through the following equation [40]:

$$B = \frac{P_{max}S}{48f}(3L^2 - 4S^2), \tag{2}$$

where B is the flexural stiffness of the beam, P_{max} the maximum fatigue load applied to the beam, L the span length of the beam, S the shear span of the beam, f the mid-span deflection under P_{max}.

Based on the Eq. (2) for the calculation of beam stiffness, the flexural stiffness degradation is defined as the normalized ratio of the beam stiffness B at certain fatigue cycle to the beam stiffness B_0 at the first static cycle. It is discovered that the stiffness degradation of SFRC beam follows the three-stage development, as shown in Fig. 11. In the first stage ($N/N_f < 10\%$), the stiffness of SFRC beam degraded rapidly. The second stage ($10\% \leq N/N_f < 90\%$) is the more stable degenerative one, the stiffness degradation of the beam is approximately proportional to the percentage of fatigue life. It is noted that when the stiffness degenerates to about 60% of the initial stiffness of each beam, the specimen enters the unstable stage ($N/N_f \geq 90\%$), the stiffness degrades quickly, and finally the failure happens. The same stiffness degradation mode was also reported for normal reinforced concrete beam [39].

The similar tendency and stages observed for the crack widths and stiffness degradation have revealed that the main effect of the added fiber can be attributed to the stiffness enhancement of the beam structures. All of the increased tensile strength of the concrete, the bonding between reinforcement and concrete, as well as the creep performance can be contributed to this stiffness enhancement. Therefore, it is possible to derive an analytical model to predict this stiffness enhancement brought by the addition of the steel fibers and convert it to a mechanism-based deflection prediction.

4. Deflection Prediction

The typical load *versus* the mid-span deflection responses for the beam, BS1.0-6, under static and fatigue loading are presented in Fig. 12. As illustrated in Fig. 12a, the deflections of the beam can be divided into two parts under fatigue load-

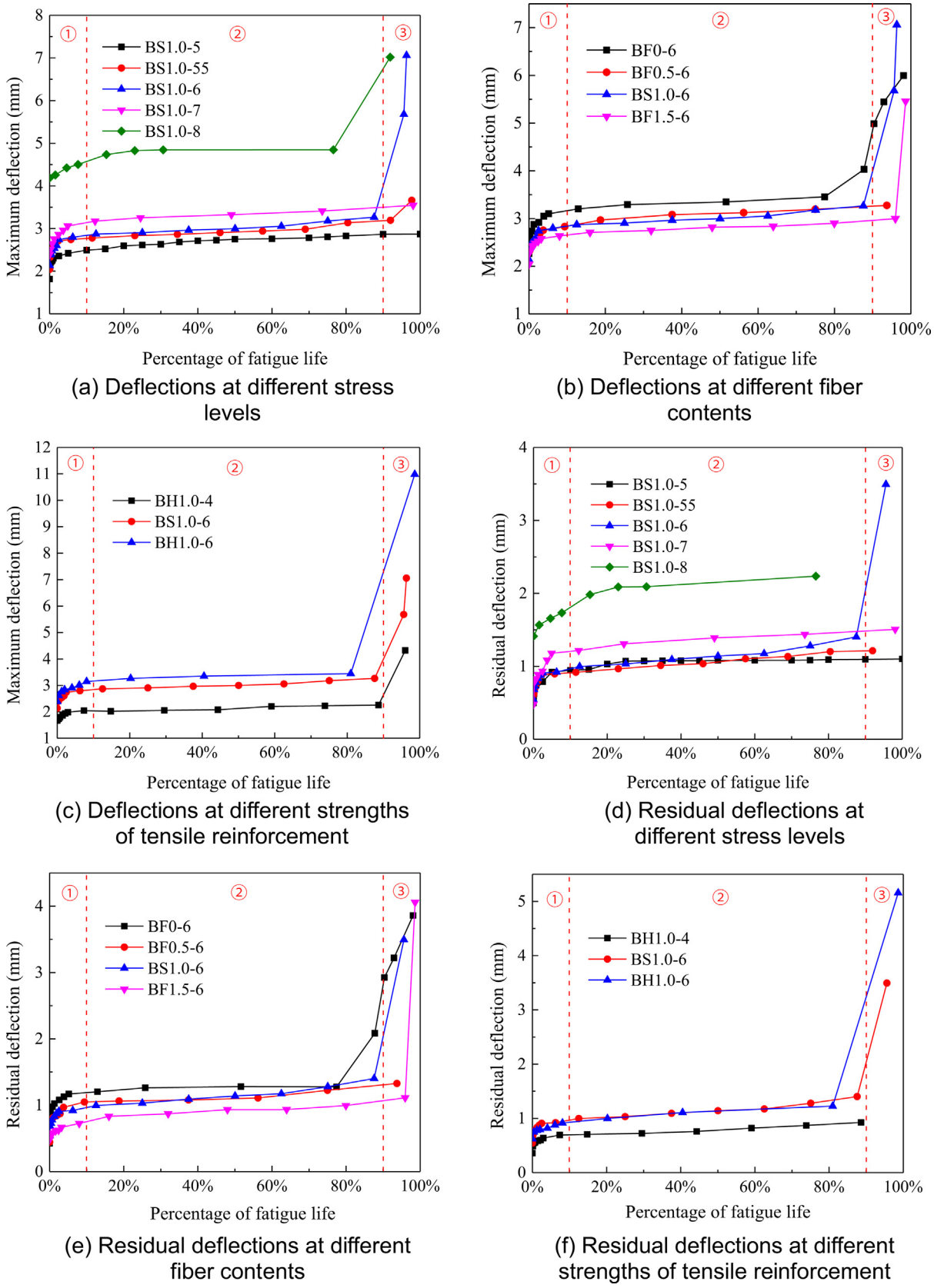

Fig. 10 – Mid-span deflections under maximum fatigue load and residual deflections versus percentage of fatigue life.

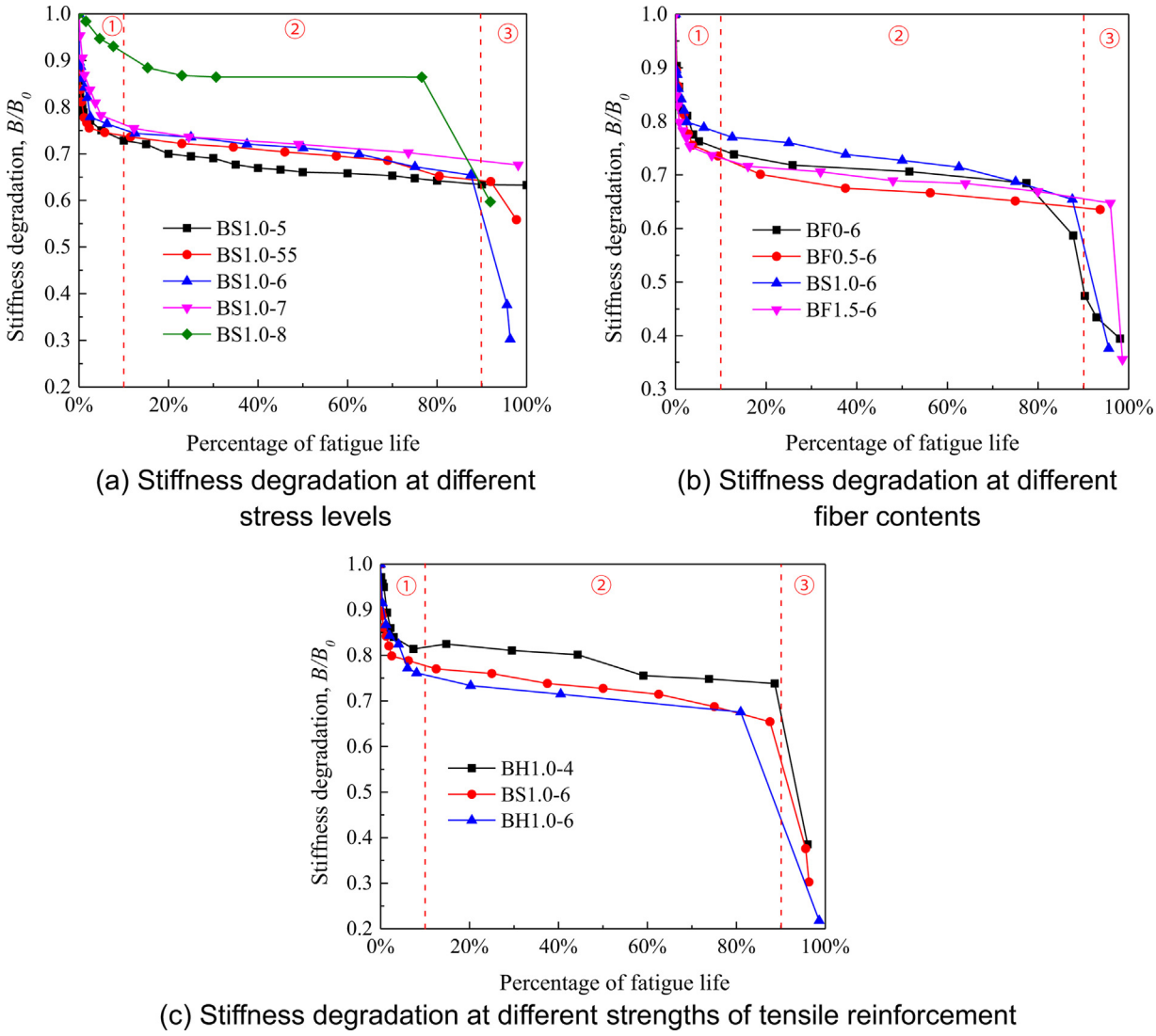

Fig. 11 – Normalized stiffness degradation versus percentage of fatigue life.

ing: residual deflection and elastic deflection [41]. The residual deflection is mainly owing to the effect of initial cracking, creep of concrete and bond slip between steel bar and concrete. The elastic deflection is due to the applied load, which is also called instantaneous deflection. In order to calculate the mid-span deflection, a diagram about the deflection analysis under fatigue loading is presented in Fig. 13.

From Fig. 13, the total deflections can be written as,

$$f_N = f_{rN} + f_{iN} \tag{3}$$

where f_N, f_{rN}, and f_{iN} are the total, residual and instantaneous deflection at N cycles, respectively. The residual deflections and instantaneous deflections are calculated through the following method respectively.

4.1. *Static deflections in the first static cycle*

According to the American Concrete Institute code, the deflection prediction of the reinforced concrete beams often uses the effective moment of inertia method. The effective moment of inertia can be calculated using the following equation [25]:

$$I_e = \left(\frac{M_{cr}}{M_a}\right)^3 I_g + \left[1 - \left(\frac{M_{cr}}{M_a}\right)^3\right] I_{cr}, \tag{4}$$

where M_{cr} is the cracking moment, M_a the maximum moment applied to the beam under fatigue loading, I_g the moment of inertia of gross section, I_{cr} the moment of inertia of cracked section.

This empirical equation is based on test data for reinforced concrete beams without fibers, which cannot be directly applied here. Zhu et al. [42] investigated the flexural behavior of partially fiber-reinforced high-strength concrete (FRHSC) beams reinforced with FRP bars, the results showed that the modified effective moment inertia method is applicable to predict the static deflections of FRHSC beams reinforced with FRP bars, whereas the steel fiber influences should be considered when calculating the moment of inertia of the beams. Therefore, the moment of inertia of gross section I_g and cracked

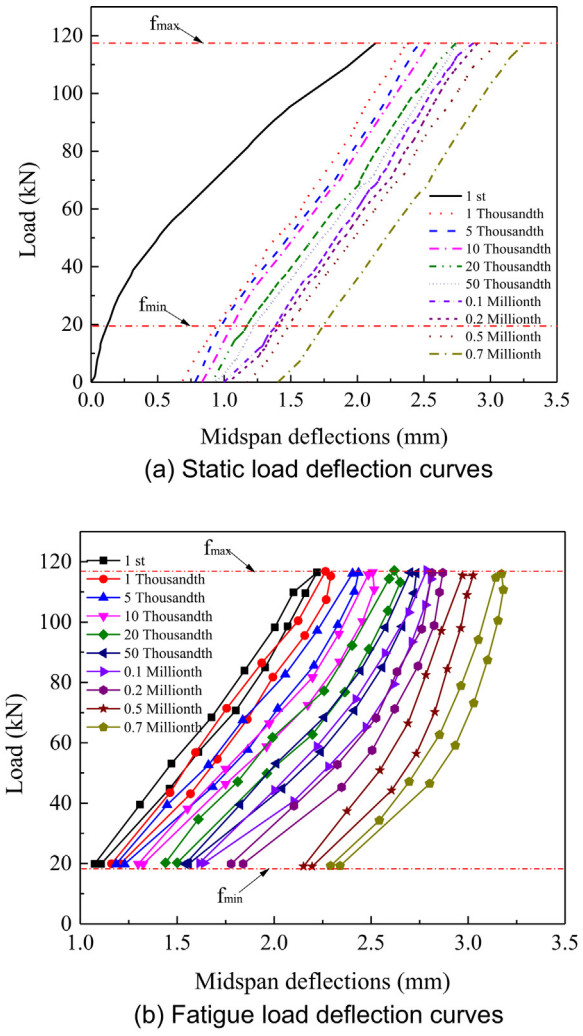

Fig. 12 – The load deflection curves at different fatigue cycles under different loading condition for BS1.0-6.

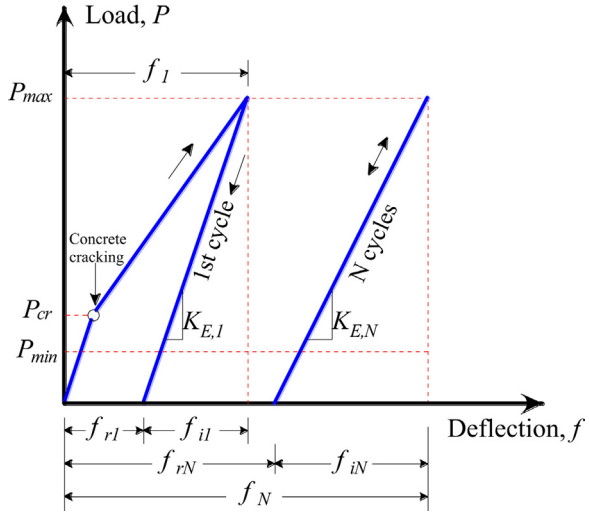

Fig. 13 – Deflections analysis of the beam under fatigue loading.

section I_{cr} of high-strength SFRC beams should be calculated using the following equations, respectively:

$$I_g = \frac{b}{3}\left[x_0^3 + (h - x_0)^3\right] + (n_s - 1)A_s(h_0 - x_0)^2 + (n'_s - 1)\,A'_s(x_0 - a'_s)^2 + \frac{n_{sf} - 1}{3h}A_{sf}\left[x_0^3 + (h - x_0)^3\right] \quad (5)$$

$$I_{cr} = \frac{bx_{cr}^3}{3} + n_s A_s(h_0 - x_{cr})^2 + (n'_s - 1)\,A'_s(x_{cr} - a'_s)^2 + \frac{n_{sf}A_{sf}(h_0 - x_{cr})^3}{3h} + \frac{(n_{sf} - 1)A_{sf}x_{cr}^3}{3h}, \quad (6)$$

where x_0 and x_{cr} are the depth of neutral axis for un-cracked and cracked section, respectively; the detailed computational process is shown in Appendix A. b and h are the width and height of beam section, respectively; $n'_s = E'_s/E_c$; $n_s = E_s/E_c$; $n_{sf} = E_f/E_c$; E'_s, E_f, and E_s are the elastic modulus of the compressive reinforcement, steel fiber, and tensile reinforcement, respectively; A'_s and A_s are the section area of compressive and tensile reinforcement, respectively; A_{sf} is the total area of steel fibers in section; a'_s is the distance between the center of compressive reinforcement and the compressive edge of beam; h_0 is the effective depth of beam. The conceptual diagrams are presented in Fig. 14.

The cracking moment of the beam can be calculated using the following equations [25]:

$$M_{cr} = \frac{f_r I_g}{y_t} \quad (7)$$

$$f_r = 0.62\lambda\sqrt{f'_c} \quad (8)$$

$$y_t = h - x_0, \quad (9)$$

where f'_c is the cylindrical compressive strength of concrete; according to the literature [43], $f'_c = 0.89f_c$, f_c is the cube compressive strength of concrete as list in Table 2; λ is the modification factor and is taken as 1.0; x_0 is the depth of neutral axis for un-cracked section.

According to Eqns. (4) to (9), the deflections of high-strength SFRC beam in the first static cycle can be calculated. Since the maximum fatigue load of the beam BS1.0-8 was 80% of its ultimate bearing capacity, the yielding of tensile reinforcement occurred in the first cycle, as well as the static beams BJ1.0-4 and BJ1.0-5. The effective moment of inertia method can only be used before the beam yield according to the American Concrete Institute code [25], hence, the experimental data of the beams BJ1.0-4, BJ1.0-5, and BS1.0-8 were not considered herein. The expression of the mid-span deflections of high-strength SFRC in the first static cycle load is given as follows:

$$f_1 = \frac{PS}{48E_c I_e}(3L^2 - 4S^2) \quad (9)$$

A close agreement was found between the predicted and experimental results as shown in Fig. 15. The average normalized ratio between the predicted and the true value, is 0.957 with a 0.059 coefficient of variation.

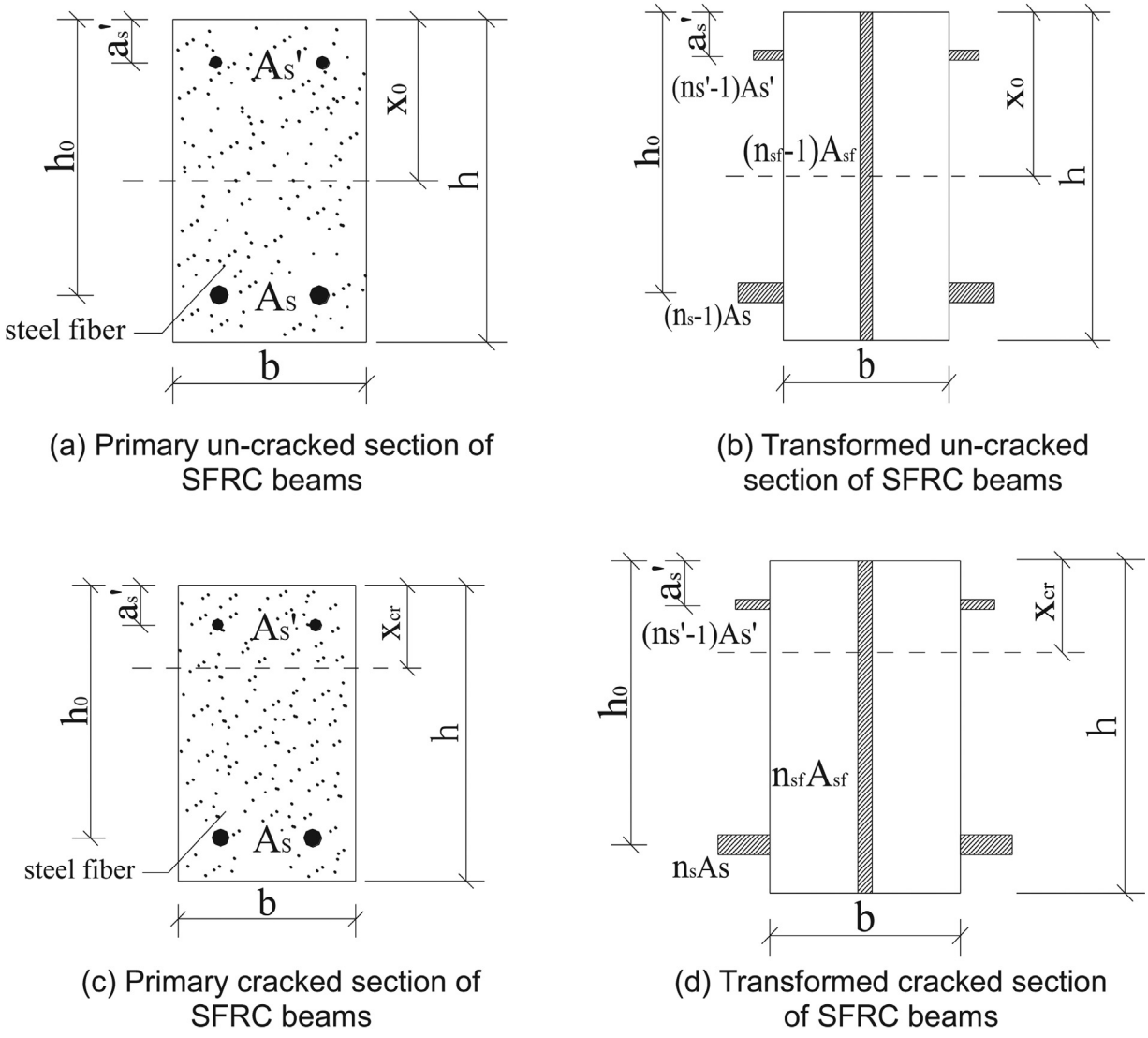

Fig. 14 – Conceptual diagram of un-cracked and cracked sections of SFRC beams.

4.2. *Residual deflection analysis*

As discussed above, the initial cracking has a significant effect on the residual deflection. Therefore, the residual deflection consists of two components. The first is the residual deflection at the first cycle ($N = 1$) due to initial cracking. The second ($N > 1$) is mainly caused by the subsequent fatigue cycles.

Existing researches [44] proposed that the residual deflections in the first cycle were closely related to the maximum fatigue bending moment, the cracking moment, the span and height of beam, and the materials properties. It can be calculated by the following equation:

$$f_{rN} = a_1 + a_2 \frac{M_a L}{M_{cr} n_s \rho h} \quad (N = 1), \tag{11}$$

where a_1 and a_2 are undetermined parameters; ρ is the tensile reinforcement ratio; L and h are the span and height of the beam, respectively.

The parameters $a_1 = -0.1826$ and $a_2 = 0.0019$ were obtained by fitting the experimental data. A close agreement is found between the predicted and experimental results, as shown in Fig. 15. The average normalized ratio between the predicted and true value, is 1.019 with a 0.064 coefficient of variation.

After the beam cracked, the creep of concrete and bond slip between steel bar and concrete were main factors that induce the increase of residual deflections under fatigue loading. The residual deflections after the first cycle ($N > 1$) are found to be almost linearly proportional with the logarithm of the fatigue life (LgN), as shown in Fig. 16. This proportional relationship remains until the beam enters the unstable stage ($N/N_f \geq 90\%$). Therefore, an empirical expression which considered the influences of beam dimensions to calculate the residual deflections after the first cycle ($N > 1$) are given as follows:

$$f_{rN} = (K_1 L_g N + K_2) \frac{L}{h} \quad (N > 1), \tag{12}$$

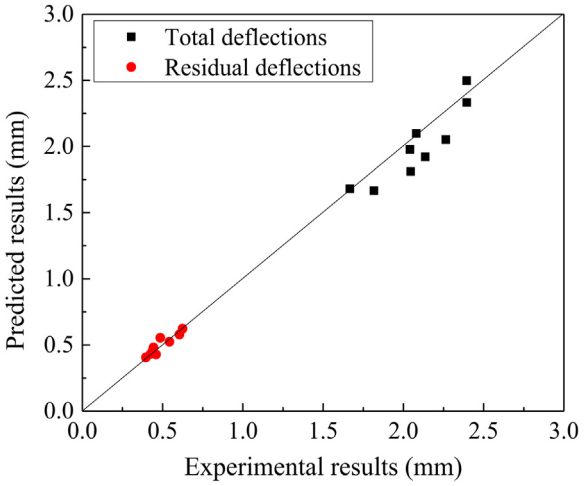

Fig. 15 – Predicted and experimental results of total deflections and residual deflections in the first static cycle load.

where K_1 and K_2 are undetermined parameters; L and h are the span and height of the beam, respectively.

Through analyzing the experimental results it is found that K_1 is mainly influenced by stress amplitude applied to the specimen and steel fiber volume fraction of the specimen, and K_2 is mainly influenced by steel fiber volume fraction. Based on the experimental data, a least-squares method was employed to fit the model. The expressions are given as follows:

$$K_1 = \left(-19.134V_f^2 + 0.394V_f + 0.0063\right) e^{3.23\Delta S} \tag{13}$$

$$K_2 = -7.376V_f + 0.0776, \tag{14}$$

where $\Delta S = S_{max} - S_{min}$; V_f is the fiber volume fraction. The residual deflections ratio between the experimental measured to the predicted at different logarithm of fatigue cycles (LgN) are presented in Fig. 17, which showed a good agreement between each other. The large deviation for beam BH1.0-4 is

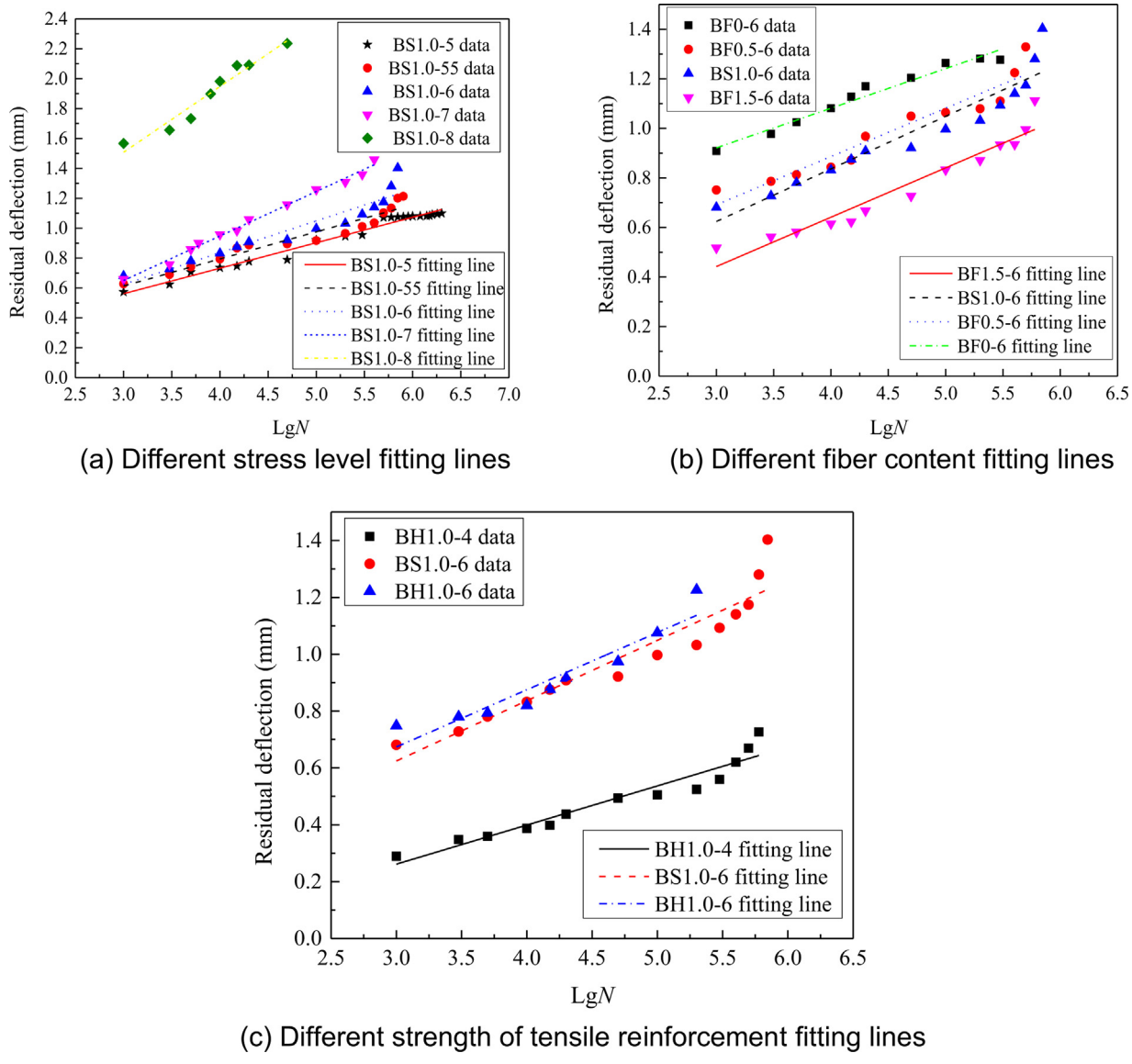

Fig. 16 – Residual deflections after the first cycle versus the logarithm of fatigue life.

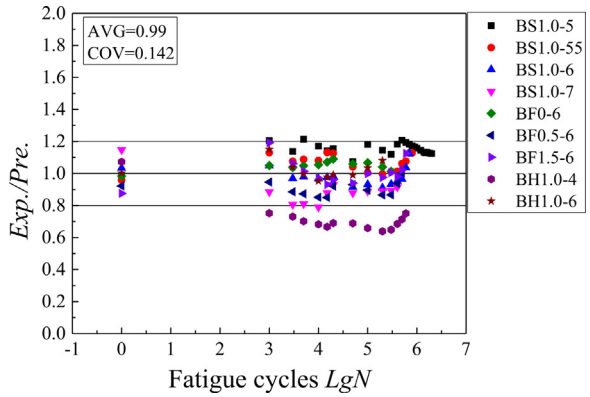

Fig. 17 – Ratio of the experimental measured residual deflections to the predicted residual deflections at different logarithm of fatigue cycles.

owing to the experimental error and the scatter of the fatigue test data.

4.3. *Instantaneous deflection calculation*

As shown in Fig. 12, the increase of residual deflection plays an important role in increasing the total deflection under fatigue loading. The instantaneous deflection is mainly contributed by the first static cycle part. The secant slope of the instantaneous deflections gradually decreases with the increase of fatigue cycles. A least-square method was employed to fit the instantaneous deflections calculated with the experimental values. According to Eq. (3), the instantaneous deflection can be calculated as follows:

$$f_{iN} = \begin{cases} f_N - f_{rN} & (N = 1) \\ 0.996N^{0.014} f_{i1} & (N > 1) \end{cases}, \tag{15}$$

where f_{i1} is the first cycle instantaneous deflection.

4.4. *Model validation*

Based on the Eqns. (3), (11), (12), and (15), the mid-span deflections of 9 high-strength SFRC beams in this experiment and 12 SFRC beams conducted by Parvez et al. [17] were calculated by the proposed model (two series beams were designed in Parvez's experiment with different specimen size). The ratio between the experimentally measured to the predicted at different logarithm of fatigue cycles (*LgN*) are presented in Fig. 18, and it showed a close agreement between the experimental measurements and calculation results.

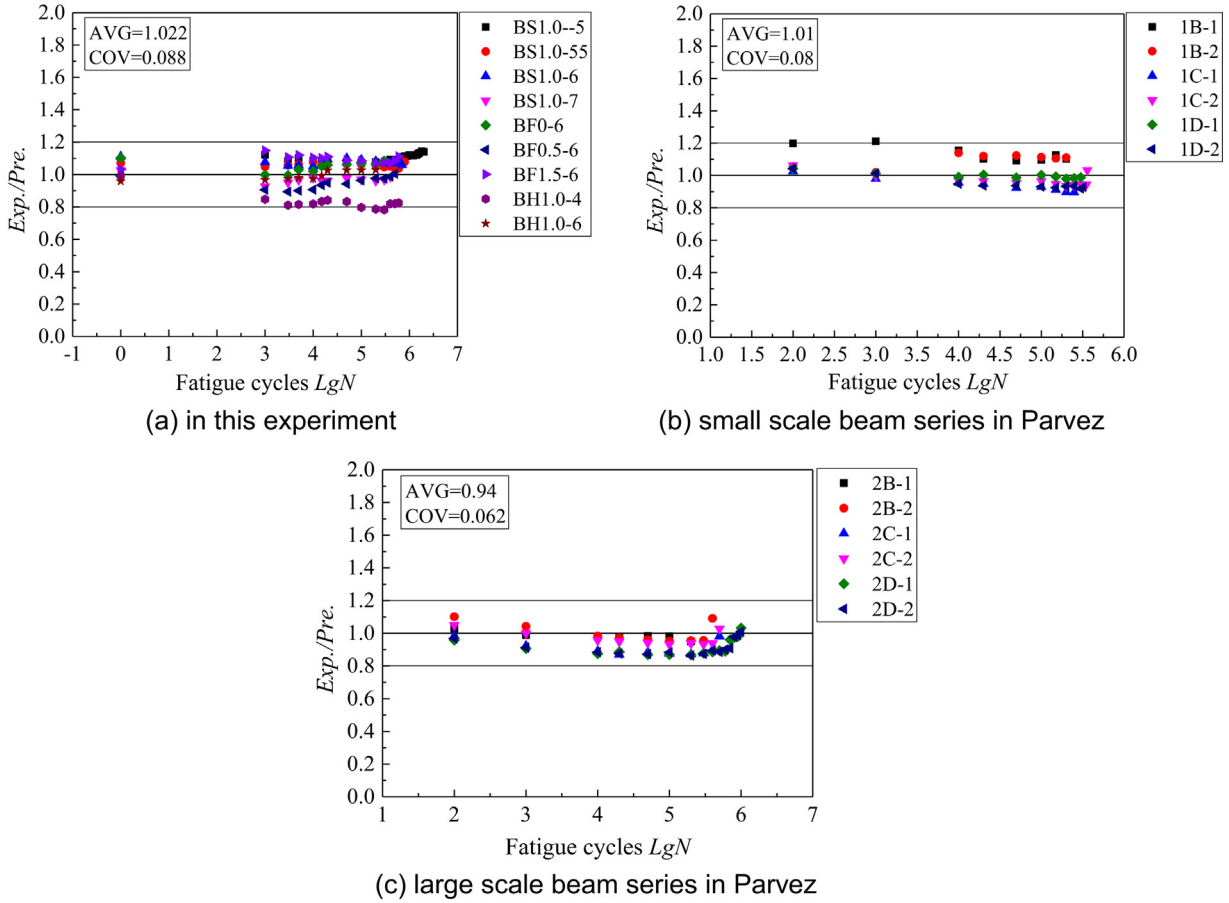

Fig. 18 – Ratio of the experimental measured mid-span deflections to the predicted mid-span deflections at different logarithm of fatigue cycles.

4.5. *Model discussion*

The deflection prediction model proposed in this paper is based on the mechanism analysis of the experimental results. The concept of residual and instantaneous deflection under fatigue loading was also proposed by other researchers [41,44], and the similar model was also used to predict the deflection [44,45] and fatigue life [46] in the open literatures, which further verified the rationality of the model. In addition, some of the equations in the model were empirically fitted, while few experimental results are available for SFRC beams subjected to fatigue loading as so far. Hence, more experimental tests are encouraged to make the further validation for the model.

5. Conclusions

The effects of stress level, steel fiber content, and tensile reinforcement strength on the fatigue performance of high-strength SFRC beam were investigated. An analytical method was proposed to predict the total and residual deflections of the beam under fatigue loading. Based on the experimental and analytical results, the following conclusions can be drawn:

- The fatigue life decreased with the increase in stress level and increased with the increase in fiber volume fraction. The strength of steel reinforcement does not show significant effect from the experimental data and observations.
- The maximum and average crack width, total and residual deflections of the beam decrease with the addition of steel fibers under fatigue load. The addition of steel fibers also significantly restrained the crack development of the beams.
- An effective moment of inertia calculation approach had been proposed to consider the effects of steel fibers. The total mid-span deflections of the beams under fatigue loading were decomposed into two components and calculated separately. The degrading stiffness of the beams was considered in this proposed analytical approach. The predicted deflections were compared with the experimental measurements. A close agreement was reached, which validated the proposed approach. This mechanism-based analytical approach provided a rational design approach for deflection behaviors of high-strength SFRC beams.

Conflict of interests

The authors claim no conflict of interests.

Acknowledgments

This research was financially supported by The National Natural Science Foundation of China (Grant No. U1704254).

Appendix A

The depth of neutral axis for un-cracked and cracked section can be obtained through the following derivation:

As shown in Fig. 14, the average distance between steel fibers and neutral axis in tensile zone and compression zone is considered 0.5 times of the depth of tension zone and compression zone, respectively. The primary and transformed un-cracked section of SFRC beams are shown in Fig. 14a and Fig. 14b. The depth of neutral axis for un-cracked section of high-strength SFRC beam can be calculated as follows:

$$\frac{bx_0^2}{2}+(n_s'-1)A_s'(x_0-a_s')+\frac{(n_{sf}-1)A_{sf}x_0^2}{2h}=\frac{b(h-x_0)^2}{2}+(n_s-1)A_s(h_0-x_0)+\frac{(n_{sf}-1)A_{sf}(h-x_0)^2}{2h} \tag{A.1}$$

$$x_0=\frac{\frac{1}{2}bh^2+(n_s'-1)A_s'a_s'+(n_s'-1)A_sh_0+\frac{1}{2}(n_{sf}-1)A_{sf}h}{(n_s'-1)A_s'+bh+(n_s-1)A_s+(n_{sf}-1)A_{sf}} \tag{A.2}$$

The total area of steel fibers in SFRC beam could be calculated through the following equation [47]:

$$A_{sf}=\eta bhV_f, \tag{A.3}$$

where V_f is steel fiber volume fraction; η is the effective coefficient of steel fibers, which is related to the distribution and orientation of steel fibers in beam section. According to Zhang [47], the value of effective coefficient η is taken as 0.33.

The primary and transformed cracked section of SFRC beams are shown in Fig. 14c and Fig. 14d. The depth of neutral axis for the cracked section of SFRC beam can be calculated as follows:

$$\frac{bx_{cr}^2}{2}+(n_s'-1)A_s'(x_{cr}-a_s')+\frac{(n_{sf}-1)A_{sf}x_{cr}^2}{2h}=n_sA_s(h_0-x_{cr})+\frac{n_{sf}A_{sf}(h-x_{cr})^2}{2h} \tag{A.4}$$

$$x_{cr}=\frac{-\left[(n_s'-1)A_s'+n_sA_s+n_{sf}A_{sf}\right]}{b-\frac{A_{sf}}{h}}+\frac{\sqrt{\left[(n_s'-1)A_s'+n_sA_s+n_{sf}A_{sf}\right]^2+2\left(b-\frac{A_{sf}}{h}\right)\left[(n_s'-1)A_s'a_s'+n_sA_sh_0+\frac{n_{sf}A_{sf}h}{2}\right]}}{b-\frac{A_{sf}}{h}} \tag{A.5}$$

REFERENCES

[1] Ding Y, Kusterle W. Comparative study of steel fibre-reinforced concrete and steel mesh-reinforced concrete at early ages in panel tests. Cem Concr Res 1999;29(11):1827–34.

[2] Ou YC, Tsai MS, Liu KY, Chang KC. Compressive behavior of steel-fiber-reinforced concrete with a high reinforcing index. J Mater Civ Eng 2011;24(2):207–15.

[3] Cánovas MF, Gaitan VH. Behavior of steel fiber high strength concrete under impact of projectiles. Mater Construcc 2012;62(307):381–96.
[4] Okay F, Engin S. Torsional behavior of steel fiber reinforced concrete beams. Constr Build Mater 2012;28(1):269–75.
[5] Wu Z, Shi C, He W, Wu L. Effects of steel fiber content and shape on mechanical properties of ultra high performance concrete. Constr Build Mater 2016;103:8–14.
[6] Yoo DY, Banthia N, Yoon YS. Impact Resistance of Reinforced Ultra-High-Performance Concrete Beams with Different Steel Fibers. ACI Struct J 2017;114(1):113–24.
[7] Ulzurrun GS, Zanuy C. Enhancement of impact performance of reinforced concrete beams without stirrups by adding steel fibers. Constr Build Mater 2017;145:166–82.
[8] Kovács I, Balázs GL. Structural behaviour of steel fibre reinforced concrete. Struct Concr 2003;4(2):57–63.
[9] Meda A, Minelli F, Plizzari GA. Flexural behaviour of RC beams in fibre reinforced concrete. Compos B Eng 2012;43(8):2930–7.
[10] Yin W, Hsu TT. Fatigue behavior of steel fiber reinforced concrete in uniaxial and biaxial compression. ACI Mater J 1995;92(1):71–81.
[11] Cachim PB, Figueiras JA, Pereira PA. Fatigue behavior of fiber-reinforced concrete in compression. Cem Concr Compos 2002;24(2):211–7.
[12] Lee MK, Barr BIG. An overview of the fatigue behaviour of plain and fibre reinforced concrete. Cem Concr Compos 2004;26(4):299–305.
[13] Zhang J, Stang H, Li VC. Experimental study on crack bridging in FRC under uniaxial fatigue tension. J Mater Civ Eng 2000;12(1):66–73.
[14] Singh SP, Kaushik SK. Fatigue strength of steel fibre reinforced concrete in flexure. Cem Concr Compos 2003;25(7):779–86.
[15] Lee JY, Shin HO, Yoo DY, Yoon YS. Structural response of steel-fiber-reinforced concrete beams under various loading rates. Eng Struct 2018;156:271–83.
[16] Gao DY, Zhang M, Zhu HT. Fatigue test and stiffness calculation of steel fiber reinforced high-strength concrete beams with reinforcements. J Build Struct 2013;34(8):142–9 (in Chinese).
[17] Parvez A, Foster SJ. Fatigue behavior of steel-fiber-reinforced concrete Beams. J Struct Eng 2015;141(4):04014117.
[18] Park KT, Kim YS, Lee JG, Shin DH. Thermal stability and mechanical properties of ultrafine grained low carbon steel. Mater Sci Eng A 2000;293(1–2):165–72.
[19] Takaki S, Kawasaki K, Kimura Y. Mechanical properties of ultra fine grained steels. J Mater Process Technol 2001;117(3):359–63.
[20] Craig RJ, Decker J, Dombrowski JL, Laurencelle R, Federovich J. Inelastic behavior of reinforced fibrous concrete. J Struct Eng 1987;113(4):802–17.
[21] Qian CX, Patnaikuni I. Properties of high-strength steel fiber-reinforced concrete beams in bending. Cem Concr Compos 1999;21(1):73–81.
[22] Lim TY, Paramasivam P, Lee SL. Behavior of reinforced steel-fiber-concrete beams in flexure. J Struct Eng 1987;113(12):2439–58.
[23] Craig RJ. Flexural behavior and design of reinforced fiber concrete members. ACI Spec Publi 1987;105: 517–64.
[24] Alsayed SH. Flexural Deflection of Reinforced Fibrous Concrete Beams. ACI Struct J 1993;90(1):72–6.
[25] ACI. Building Code Requirements for Structural Concrete (ACI 318M-11) and Commentary. Farmington Hills, MI: ACI 318M-11; 2011. p. 128.
[26] CEB-FIP. Model code 2010. Comite Euro-International du beton; 2010.
[27] Parvez A, Foster SJ. 2013Numerical modelling of steel fibre reinforced concrete beams subjected to fatigue loading. In: Proceedings of the 2013 world Congress on advances in structural engineering and mechanics. 2013 Sept. p. 3109–19.
[28] Ye DY, Ping DH, Wang ZL, Xu HH, Mei XY, Xu CW, et al. Low cycle fatigue behavior of nickel-based superalloy GH4145/SQ at elevated temperature. Mater. Sci. Eng 2004;373:54–64.
[29] Yadollahi A, Shamsaei N, Thompson SM, Elwany A, Bian L. Effects of building orientation and heat treatment on fatigue behavior of selective laser melted 17-4 PH stainless steel. Int J Fatigue 2017;94:218–35.
[30] Hou ZJ, Chen SY, Sun QY, Wei XS, Lv W. Experimental research on fatigue characteristics of X12Cr13 stainless steel. J Mater Res Tec 2020.
[31] Travieso-Rodríguez JA, Jerez-Mesa R, Gómez-Gras G, Llumà-Fuentes J, Casadesús-Farràs O, Madueño-Guerrero M. Hardening effect and fatigue behavior enhancement through ball burnishing on AISI 1038. J Mater Res Tec 2019.
[32] Tan KH, Paramasivam P, Tan KC. Cracking characteristics of reinforced steel fiber concrete beams under short-and long-term loadings. Adv Cem Based Mater 1995;2(4):127–37.
[33] Gali S, Subramaniam KV. Investigation of the dilatant behavior of cracks in the shear response of steel fiber reinforced concrete beams. Eng Struct 2017;152:832–42.
[34] Holmen JO. Fatigue of concrete by constant and variable amplitude loading. ACI Special Publication 1982;75:71–110.
[35] Li Q, Huang B, Xu S, Zhou B, Rena CY. Compressive fatigue damage and failure mechanism of fiber reinforced cementitious material with high ductility. Cem Concr Compos 2016;90:174–83.
[36] Branco R, Costa JD, Antunes FV. Low-cycle fatigue behaviour of 34CrNiMo6 high strength steel. Theo App Frac 2012;58:28–34.
[37] Yadollahia A, Mahmoudi M, Elwany A, Doude H, Biana L, Newman JC. Effects of crack orientation and heat treatment on fatigue-crack growth behavior of AM 17-4 PH stainless steel. Eng Fract Mech 2020;226:106874.
[38] Zanuy C, Fuente P, Albajar L. Effect of fatigue degradation of the compression zone of concrete in reinforced concrete sections. Eng Struct 2007;29(11):2908–20.
[39] Zanuy C, Albajar L, Fuente P. Sectional analysis of concrete structures under fatigue loading. ACI Struct J 2009;106(5):667–77.
[40] Mousavi SR, Esfahani MR. Effective Moment of Inertia Prediction of FRP-Reinforced Concrete Beams Based on Experimental Results. J Compos Constr 2012;16(5):490–8.
[41] Chen HJ, Liu TH, Tang CW. Pre-failure deflection and residual load capacity of reinforced lightweight aggregate concrete beams under high-cycle fatigue. Adv Mat Res 2011;146:926–36.
[42] Zhu H, Cheng S, Gao D, Neaz SM, Li C. Flexural behavior of partially fiber-reinforced high-strength concrete beams reinforced with FRP bars. Constr Build Mater 2018;161:587–97.
[43] Guo ZH. Theory of reinforced concrete. 3nd. ed Beijing: Tsinghua university press; 2012 (in Chinese).
[44] Song A, Wan S, Jiang Z, Xu J. Residual deflection analysis in negative moment regions of steel-concrete composite beams under fatigue loading. Constr Build Mater 2018;158:50–60.
[45] Song YP. Fatigue behavior and design principle of concrete structures. Beijing: China Machine Press; 2006 (in Chinese).
[46] Yadollahi A, Mahmoudi M, Elwany A, Doude H, Bian L, Newman JC. Fatigue-life prediction of additively manufactured material: Effects of heat treatment and build orientation. Fatigue Fract Eng M 2020:1–14.
[47] Zhang M. Fatigue performance and calculation method of steel fiber reinforced High-strength concrete beams [Ph.D. dissertation]. Zhengzhou: Zhengzhou University; 2015 (in Chinese).